Accepted Manuscript

Exploiting multi-function Metal-Organic Framework Nanocomposite Ag@Zn-TSA as highly efficient immobilization matrixes for sensitive electrochemical biosensing

Sheying Dong, Dandan Zhang, Gaochao Suo, Wenbo Wei, Tinglin Huang

PII: S0003-2670(16)30715-2

DOI: 10.1016/j.aca.2016.05.040

Reference: ACA 234606

To appear in: *Analytica Chimica Acta*

Received Date: 20 March 2016

Revised Date: 18 May 2016

Accepted Date: 23 May 2016

Please cite this article as: S. Dong, D. Zhang, G. Suo, W. Wei, T. Huang, Exploiting multi-function Metal-Organic Framework Nanocomposite Ag@Zn-TSA as highly efficient immobilization matrixes for sensitive electrochemical biosensing, *Analytica Chimica Acta* (2016), doi: 10.1016/j.aca.2016.05.040.

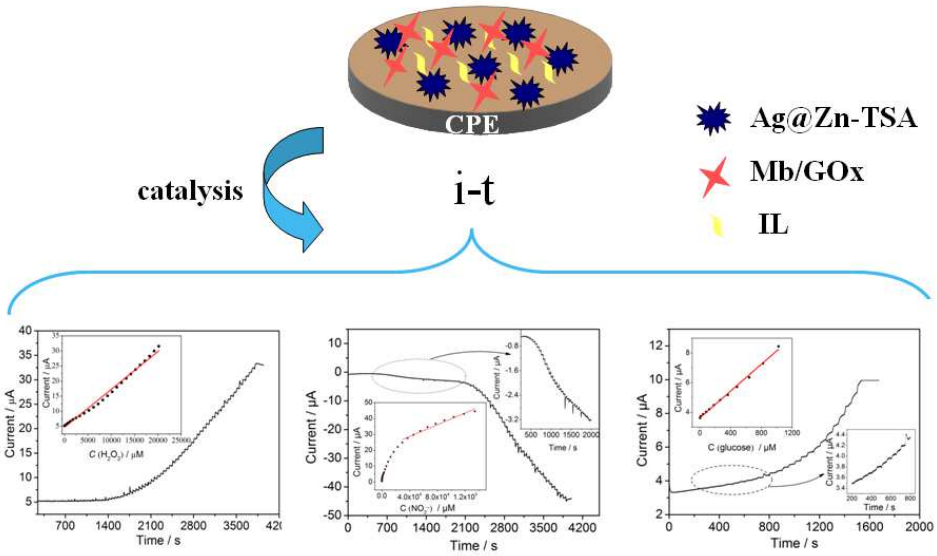

Exploiting multi-function Metal-Organic Framework Nanocomposite Ag@Zn-TSA as highly efficient immobilization matrixes for sensitive electrochemical biosensing

Sheying Dong [a,*], Dandan Zhang [a], Gaochao Suo [a], Wenbo Wei [a], Tinglin Huang [b]

[a] *College of Sciences, Xi'an University of Architecture and Technology, Xi'an, 710055, China*

[b] *School of Environmental and Municipal Engineering, Xi'an University of Architecture and Technology, Xi'an 710055, China*

*Corresponding author. Tel.: +86 29 82201203; fax: +86 29 82205332.

E-mail address: dongsyy@126.com (S.Y. Dong)

Abstract

A novel multi-function Metal-Organic Framework composite Ag@Zn-TSA (zinc thiosalicylate, $Zn(C_7H_4O_2S)$, Zn-TSA) was synthesized as highly efficient immobilization matrixes of myoglobin (Mb)/glucose oxidase (GOx) for electrochemical biosensing. The electrochemical biosensors based on Ag@Zn-TSA composite and ionic liquid (IL) modified carbon paste electrode (CPE) were fabricated successfully. Furthermore, the properties of the sensors were discussed by cyclic voltammetry (CV), electrochemical impedance spectroscopy (EIS) and amperometric current-time curve, respectively. The results showed the proposed biosensors had wide linear response to hydrogen peroxide (H_2O_2) in the range of 0.3-20000 μM, to nitrite (NO_2^-) for 1.3 μM -1660 μM and 2262 μM -133000 μM, to glucose for 2.0-1022 μM, with a low detection limit of 0.08 μM for H_2O_2, 0.5 μM for NO_2^-, 0.8 μM for glucose. The values of the apparent heterogeneous electron transfer

rate constant (k_s) for Mb and GOx were estimated as 2.05 s^{-1} and 2.45 s^{-1}, respectively. Thus, Ag@Zn-TSA was a kind of ideal material as highly efficient immobilization matrixes for sensitive electrochemical biosensing. In addition, this work indicated that MOF nanocomposite had a great potential for constructing wide range of sensing interface.

Keywords: Metal-Organic Framework, Ag@Zn-TSA, myoglobin/glucose oxidase, Ionic liquid, Biosensor

Introduction

The electrochemical behaviors of redox electroactive proteins and enzymes such as hemoglobin (Hb), myoglobin (Mb), glucose oxidase (GOx), cytochrome c (Cyt C) and horseradish peroxidase (HRP) on different kinds of modified electrodes have been reported, which can be used in the construction of third generation electrochemical biosensors [1-2]. For example, Sheying Dong et al. [3] studied a simple and reliable method for the electrochemical determination of nitrite based on the immobilization of myoglobin (Mb) on LaF_3 doped CeO_2 (LaF_3-DP-CeO_2) and ionic liquid (IL) composite film. Yunxian Piao et al. [4] constructed a glucose enzyme biosensor and immobilized the glucose oxidase (GOx) on the Graphite nanoparticle (GN), where the surface of the GN was first modified by 1-pyrenebutyric acid N-hydroxysuccinimide ester (Py-NHS ester) by π-π stacking interaction between the pyrene moiety and the GN to produce the GN-Py-NHS ester conjugates, and then the GOx was linked with GN-Py-NHS ester through amide bond. Lu et al. [5] investigated the direct

electrochemistry of HRP in a composite system based on chitosan and 1-butyl-3-methylimidazolium tetrafluoroborate. However, sensitivity, stability and reproducibility for the electrochemical biosensors of redox electroactive proteins and enzymes need to improve. In addition, we expect to construct a wide range of sensing interface by exploiting a variety of functions of materials.

Recently, Metal-organic Frameworks (MOFs), constituted by a three dimensional array of metal ions or metal clusters connected by rigid bi- or multipodal organic linkers [6], have developed rapidly with fantastic potential applications covering different areas including energy, environment, material and biology [7-8]. Base on the properties of these materials such as high specific surface areas, porosity, structural diversity, controllable synthesis, rich metal active site and flexibility of the pore size/wall modification, several research groups are trying to apply MOFs as electrode materials to develop electrochemical methods with high sensitivity and selectivity for efficiently detecting trace amount of biologically related compounds [9-12].

Most of MOF modified electrodes as sensors are based on the post-modified method such as linking -NH_2 or -SH functional groups and doping other dopants [13-14]. For instance, Vasiliki Lykourinou et al. [15] demonstrated the successful immobilization and characterization of microperoxidase-11 (MP-11) into a mesoporous MOF, resulting that MP-11@mesoMOF exhibited superior enzymatic catalysis performances compared to the mesoporous silica counterpart. Hadi Hosseini et al. [16] prepared SH-SiO_2 by the hydrolysis of 3 - (trimethylsilyl) - 1 -propyl mercaptan on the surface of the SiO_2 nanoparticles, Au-SH-SiO_2@Cu-MOF was

subsequently prepared by the reaction of trimesic acid, SH-SiO_2 with $Cu(NO_3)_2$, and the adsorption of gold nanoparticles. The electrochemical sensor for the determination of L-cysteine based on Au-SH-SiO_2@Cu-MOF showed a stronger electrocatalytic oxidation activity to L - cysteine, with a detection limit of 0.008 μM.

It is noteworthy that the conjugate structure of thiosalicylic acid (TSA) makes it full of delocalized electrons, Zn-TSA may accelerate the interfacial electron transfer. At the same time, the existence of carboxyl and thiol groups in the TSA is beneficial for the immobilization of proteins/enzyme. In addition, the Ag nanoparticles have shown some advantages such as enhancement of mass and electron transport, high effective surface area, high conductivity and specially improvement of nano diamond graphite (NDG) dispersion in the solvent due to impediment of NDG aggregation [17]. Saeed Shahrokhian et al. [18] prepared Ag nanoparticles decorated NDG modified electrode for voltammetric determination of ceftizoxime, and the prepared modified electrode has some remarkable electrochemical properties such as high sensitivity, excellent repeatability and reproducibility and long-term stability. It should be noted that, the excellent biocompatibility and interface dominated properties of Ag nanostructures have stimulated an increasing interest in designing novel and high-performance electrochemical biosensing devices [19]. All the above provide a basis for the research of electrochemical sensors. With this in mind, we prepared a new composite material, which has good electrochemical performance due to the synergistic effect of silver and Zn-TSA.

Herein, a novel multi-function Metal-Organic Framework composite

(Ag@Zn-TSA) was synthesized by Microwave and Chemical reduction method. Myoglobin (Mb)/Glucose Oxidase (GOx) were incorporated within Ag@Zn-TSA and ionic liquid 1-ethyl-3-methylimidazolium tetrafluoroborate ([BMIm]BF_4) composite films to fabricate modified carbon paste electrode (CPE). The composition and morphology of Ag@Zn-TSA composite and modified electrodes were investigated by Fourier transform infrared spectrometry (FT-IR), UV-visible spectroscopy (UV-vis), Scanning electron microscopy (SEM), Energy Dispersive Spectrometer (EDS), and X-ray diffraction (XRD). Furthermore, the properties of the electrochemical sensor were discussed by cyclic voltammetry (CV) and electrochemical impedance spectroscopy (EIS). Furthermore, electrochemical catalytic ability of Mb/Ag@Zn-TSA/IL-CPE and GOx/ Ag@Zn-TSA/IL-CPE to hydrogen peroxide (H_2O_2), sodium nitrite ($NaNO_2$) and glucose were also investigated.

2. Experimental

2.1 Reagents and apparatus

Glucose oxidase (GOx, MW 15 0000) was purchased from Aladdin Reagent co., LTD, Bovine myoglobin (Mb, MW 17 800) was purchased from Sigma Chemical Co., H_2O_2 was purchased from Aladdin Reagent co., LTD. Glucose was purchased from Aladdin Reagent co., LTD. 1-butyl-3-methylimidazolium tetrafluoroborate [BMIm]BF_4 (IL) was purchased from Hangzhou Chemer Chemical Limited Company. All the chemicals were of analytical reagent grade and used without further purification.

Metal-Organic Frameworks composite (Ag@Zn-TSA) was analyzed by scanning electron microscopy (SEM; QUANTA650F, American). UV-vis spectra were recorded on a Nicolet Evolution 300 spectrophotometer in 0.1 M PBS and the IR spectra (KBr) were recorded on an IR-spectrometer FTIR-21 Shimadzu at room temperature. The X-ray diffraction (XRD) measurements were carried out on the D8-Advance X-ray diffractometer using monochromatic Cu Kα radiation.

2.2 The synthesis of Zn-TSA and Ag@Zn-TSA framework composite

The synthesis process of Zn-TSA is based on the reference [20]. The detail description of this part was described in the supplementary material. The schematic diagram of the procedure to synthesize Zn-TSA and Ag@Zn-TSA framework composite was shown in Scheme 1.

Scheme 1. here

2.3 Preparation of the Modified Electrode

The Mb modified electrode was prepared according to the following procedures: 5.0 mg Ag@Zn-TSA, 5.0 mg Mb and 10 μL IL ($[BMIm]BF_4$) were dispersed into 1 mL anhydrous ethanol, 1.0 mL 0.1 M pH 7.0 PBS and 1.0 mL 0.1 M pH 7.0 PBS by ultrasonic agitation, respectively. First, 5 μL of Ag@Zn-TSA solution (5.0 $mg \cdot mL^{-1}$) was casted onto the surface of a freshly polished CPE to obtain Ag@Zn-TSA-CPE, which was dried at room temperature to form a stable film. Second, Mb/Ag@Zn-TSA/IL-CPE was prepared by casting 5 μL Mb solution (5 $mg \cdot mL^{-1}$) and 5 μL IL onto the Ag@Zn-TSA-CPE, respectively, which was subsequently evaporated

in a refrigerator at 4 □ to form a stable film. Finally, the modified electrode was rinsed twice or thrice with doubly distilled water to remove the unimmobilized Mb molecules. It's noteworthy that the electrode needs to be activated in 0.1 M PBS (pH 7.0) solution by cyclic voltammetry (CV) until a stable blank background was obtained in the potential range from -0.8 V to 1.0 V at a scan rate of 100 $mV \cdot s^{-1}$. The enzyme electrodes were stored in 0.1 M pH 7.0 PBS at 4 □ in a refrigerator when not in use.

The fabrication of the GOx modified electrode (GOx/Ag@Zn-TSA/IL-CPE) was similar to that of Mb/Ag@Zn-TSA/IL-CPE.

2.4 Electrochemical Measurements

The detail description of this part was described in the supplementary material.

3. Results and discussion

3.1 Characterization of Ag@Zn-TSA

Fig. 1. here

The important functional groups information of the compound can be investigated by Fourier transform infrared spectroscopy (FT-IR). **Fig. 1A** displays the FT-IR spectroscopy of Zn-TSA and TSA, respectively. The absorption peak at 3400 cm^{-1} was attributed to the absorption of -OH, meanwhile, the absorption peak at around 1700 cm^{-1} was due to the absorption of C=O in Zn-TSA and in the ligand TSA. The absorption peak at 2500 cm^{-1} (TSA curve) was result from the -SH in the TSA,

while the absorption peak at 2500 cm^{-1} (Zn-TSA curve) disappeared, indicating that the -SH participated in the coordination with Zn when the frame structure formed. At the same time, the absorption peak at 460 cm^{-1} (Zn-TSA curve) was the characteristic absorption peak of Zn-O, indicating that the -COOH of TSA was involved in the coordination with Zn, and the absorption peak of Zn-S appeared at 724 cm^{-1} [21]. It is concluded that the -SH and -COOH in the TSA simultaneously participated in the coordination with Zn when the frame structure formed.

The powder X-ray diffraction (XRD) pattern shown in **Fig. 1B** was used to confirm the phase structure of the Ag particle and the Zn-TSA of the Ag@Zn-TSA samples prepared in this work. The intensive peaks (38.26°, 44.47°, 64.71°, 77.74°, 81.91°) appeared at small 2θ angles are characteristics of Ag particle, which are in accordance with silver standard card (PDF# 04-0783), indicating the Ag particles were successfully composited with Zn-TSA by chemical reduction method at room temperature [22]. In addition, the other intensive peaks (31.84°, 33.40°, 34.61°, 36.42°, 47.75°, 56.81°, 59.67°, 62.99°, 68.13°) appeared at small 2θ angles are characteristics of Zn-TSA, which are coincident with previously published results [23].

The morphology of as-prepared Zn-TSA and Ag@Zn-TSA were characterized by field emission scanning electron microscopy (FE-SEM). As shown in **Fig. 1C**, it can be seen that Zn-TSA(**C1**) was composed of regularly cuboid-like or flake with a relatively loose structure, and cascading into layered with length around 1 μm, and the particle size of Zn-TSA in the range of 0.5-11 μm. While the Ag@Zn-TSA (**C2**) presented a relatively uniform particles with no obvious agglomeration, and the

material was well-dispersed with an average size about 100 nm, which also suggested that Ag particles were composited with Zn-TSA successfully.

In order to confirm whether the Ag particles were composited with Zn-TSA, Energy Dispersive Spectrometer (EDS) measurements were used to analyze the elemental composition of the composite. As shown in **Fig. 1D**, Ag@Zn-TSA composite contains 11.72%, 16.48%, 2.12%, 61.69% and 7.99% of C, O, S, Zn and Ag, respectively, indicating that Ag particles were successfully combined with Zn-TSA and formed functional Ag@Zn-TSA particles.

3.2 Characterization of the Electrodes Modified by Zn-TSA and Ag@Zn-TSA

Modified electrodes of Zn-TSA and Ag@Zn-TSA were investigated by UV-visible spectroscopy (UV-vis) and Scanning electron microscopy (SEM), which indicating that the Ag@Zn-TSA with good biocompatibility and protein/enzyme was successfully immobilized on the surface of the underlying electrode. The detail description of this part was shown in the supplementary material.

3.3 Electrochemical performance of Ag@Zn-TSA

Fig.2. here

Electrochemical impedance spectrum (EIS) can effectively provide impedance change information in the process of modifying on the surface of electrode [24], which were carried out in 5.0 mM $K_3Fe(CN)_6/K_4Fe(CN)_6$ (1:1) containing 0.1 M KCl, as shown in **Fig. 2**. Electronic transfer resistance (R_{et}) can be determined by calculating

the diameter of the high-frequency semicircle in the Nyquist curve [25]. It could be observed that the R_{et} of Ag@Zn-TSA-CPE (**Fig. 2A**) was smallest, suggesting Ag@Zn-MOF played the role of electron channel. The R_{et} of the modified electrodes obviously increased to 3500 ohm when Mb was immobilized on the Ag@Zn-TSA-CPE. It was because that dielectric behavior of enzyme molecules would result in a higher barrier for interfacial electron transfer, confirming that Mb had been successfully immobilized on the surface of Ag@Zn-TSA-CPE and blocked the electron exchange between the redox probe and the electrode. Obviously, the high conductive BmimBr (IL) contributed to a lower R_{et} of Mb/Ag@Zn-TSA/IL-CPE. In the meantime, the film of IL formed could wrap proteins and prevent them fall off. An analogous result also appeared to be in **Fig. 2B**, confirming that protein/enzyme had been successfully immobilized on the surface of Ag@Zn-TSA-CPE. As shown in **Fig.2B**, the R_{et} of Ag@Zn-TSA-CPE was obviously smaller than that of Zn-TSA-CPE, suggesting that Ag accelerated the electron transfer. It also indicated that Ag@Zn-TSA was successfully synthesized, which was consistent with its morphology characterization.

3.4 Direct Electrochemistry of the Mb/GOx Modified Electrodes

Fig. 3. here

As shown in **Fig. 3**, the electrochemical behaviors of different Mb and GOx modified electrodes were characterized by cyclic voltammetry (CVs) in 0.1 M PBS (pH 7.0) at a scan rate of 0.1 $V \cdot s^{-1}$. Compared to CPE, Mb/IL-CPE and

Mb/Zn-TSA/IL-CPE, the CVs data demonstrated that the Mb/Ag@Zn-TSA/IL-CPE (Fig.3A-d, Fig.3B-d') in our experimental conditions was best to the direct electron transfer of Mb/GOx. Apparently, a pair of stable and well-defined redox peaks appeared with good reversibilities, and its peak current value increased significantly, indicating that Ag@Zn-TSA can effectively immobilize Mb/GOx and facilitate the direct electron transfer between Mb/GOx and underlying electrode. The Zn-TSA with large specific surface area, high porosity, good adsorption performance can absorb more protein molecules, and the existence of carboxyl and thiol groups in the TSA itself is beneficial for the immobilization of proteins/enzyme. On the other hand, synergistic effect of silver and the conjugate structure of TSA with delocalized electrons make it exhibit an excellent conductivity, which can accelerate the interfacial electron transfer.

3.5 The kinetic parameters

Fig. 4. here

The CVs of Mb/Ag@Zn-TSA/IL-CPE and GOx/Ag@Zn-TSA/IL-CPE at different scan rates were shown in **Fig. 4**, respectively. As shown in **Fig. 4A** and **Fig.4B**, the anodic and cathodic peak currents increased with the increase of scan rates from 0.02 to 1.00 $V \cdot s^{-1}$, and the oxidation peaks shifted to more positive potentials and the reduction peaks shifted to more negative potentials. For Mb/Ag@Zn-TSA/IL-CPE, the peak currents **(i_p)** were proportional to the square root of the scan rate ($v^{1/2}$) ($i_{p,a}$=−2.933$v^{1/2}$+16.386 (R=0.9966), $i_{p,c}$=2.672$v^{1/2}$−1.203

(R=0.9996)). The anodic and cathodic peak currents increased linearly with the scan rates (v) in the range of 0.15~0.5V·s^{-1} ($i_{p,a}$= − 0.0846v − 6.611 (R=0.9983), $i_{p,c}$=0.07987v + 22.467 (R=0.9946)). For GOx/Ag@Zn-TSA/IL-CPE, the peak currents (i_p) were proportional to the v ($i_{p,a}$=63.73v+9.51 (R=0.9971), $i_{p,c}$=−74.54v −2.865(R=0.9962)). The anodic and cathodic peak currents were proportional to the $v^{1/2}$ in the range of 0.4 ~ 1.0 V·s^{-1} ($i_{p,a}$=−107.780$v^{1/2}$+34.033 (R=0.9991), $i_{p,c}$= 90.262$v^{1/2}$−20.445 (R=0.9997)), suggesting that the electrochemical reactions of the modified electrode Mb/Ag@Zn-TSA/IL-CPE and GOx/Ag@Zn-TSA/IL-CPE were both surface-controlled process whose surface reactions were accompanied by the adsorption process with the scan rates in the range of 0.15 ~ 0.5 V·s^{-1} and the diffusion process at high scan rates [26].

For a surface-controlled process, integration of reduction peaks gave nearly constant charge (Q) value with different scan rates. The average surface coverage (Γ*) of electroactive Mb/GOx on the modified electrode was estimated at slow scan rates according to the Faraday's law [27] Q= nFAΓ*. Where Q is the charge involved in the reaction, n is electron transfer number, F is Faraday's constant, and A is the effective surface area of electrode. The number of electron transferred for Mb is 1 and 2 for GOx, the value of Γ* were calculated as 1.528×10^{-11} M·cm^{-2} and 1.737×10^{-11} M·cm^{-2} for Mb/Ag@Zn-TSA/IL-CPE and GOx/Ag@Zn-TSA/IL-CPE, respectively. The results above suggested that Mb/GOx can be immobilized into the Ag@Zn-TSA/IL composite film and the Ag@Zn-TSA composite with good biocompatibility can provide a suitable microenvironment for the immobilization of Mb/GOx.

The oxidation peak potentials at Mb/Ag@Zn-TSA/IL-CPE and GOx/Ag@Zn-TSA/IL-CPE both slightly shifted to the positive direction and the reduction peak potentials to the negative direction with the increase of the scan rates. For the surface-controlled progress, Laviron's Equation [28] could be expressed as follows:

$$E_{p,a} = E^{0'} + RT\ln v / (1-\alpha)nF \quad (1)$$

$$E_{p,c} = E^{0'} - RT\ln v / \alpha nF \quad (2)$$

$$\log k_s = \alpha\log(1-\alpha) + (1-\alpha)\log\alpha - \log(RT/nFv) - (1-\alpha)\alpha nF\Delta E_p/2.3RT \quad (3)$$

Where α is the electron transfer coefficient, n is the number of electron transfer, F is Faraday's constant, k_s is the heterogeneous electron transfer rate constant. As shown in **Fig. 4A'**, the peak potentials had a linear relationship *vs.* the ln*v* in the range of 0.45 – 1.00V·s^{-1} with the equations as $E_{p,a}$=0.0778ln*v*－0.635 (*R*=0.9935) and $E_{p,c}$=－0.1002ln*v*－0.1001 (*R*=0.9847)). As shown in **Fig. 4B'**, the peak potentials had a linear relationship *vs.* the ln*v* in the range of 0.36 – 1.00V·s^{-1} with the equations as ($E_{p,a}$=0.0289ln*v*－0.4304 (*R*=0.9946), $E_{p,c}$=－0.0367ln*v*－0.5733 (*R*=0.9952)). The values of electron transfer coefficient (α) and the apparent heterogeneous electron transfer rate constant (k_s) were estimated as 0.48 and 2.05 s^{-1}, 0.58 and 2.45 s^{-1} for Mb/Ag@Zn-TSA/IL-CPE and GOx/Ag@Zn-TSA/IL-CPE, respectively. The larger k_s value showed that the electron shuttling between redox active sites of Mb/GOx and the underlying electrode surface was faster in Ag@Zn-TSA/IL-CPE, which could be ascribed to the high conductivity of the Ag@Zn-TSA/IL composite film.

3.6 Electrocatalytic activity of Mb/GOx modified electrodes

Fig. 5. here

As shown in **Fig. 5,** the catalytic behavior of the modified electrode was investigated by cyclic voltammetry (CVs) and amperometric current-time response curves, respectively. **Fig. 5A** and **Fig. 5B** were the CVs of Mb/Ag@Zn-TSA/IL-CPE at different concentrations of H_2O_2 and NO_2^-, respectively. When H_2O_2 was added to the 0.1 M pH 7.0 PBS at scan rate 100 $mV \cdot s^{-1}$, an increase in reduction peak at about -0.35 V was observed with the disappearance of the oxidation peak for Mb Fe(II). The reduction peak current increased with the increase of concentration of H_2O_2 in solution. When NO_2^- was added to the 0.1 M pH 7.0 PBS at scan rate 100 $mV \cdot s^{-1}$, an increase in oxidation peak at about 0.8 V was observed. The oxidation peak current increased with the increase of concentration of NO_2^- in solution, which indicated that the modified electrode had an obvious catalytic effect on H_2O_2 and NO_2^-. **Fig. 5C** was the CVs of GOx/Ag@Zn-TSA/IL-CPE in an N_2-saturated phosphate buffer solution (0.1 M, pH = 7.0) containing different concentrations of glucose. It is clearly seen that the redox peak currents decreased with the increase of glucose concentration, which was the typical trend for glucose oxidase catalyzing glucose, indicating that the GOx modified electrode had an obvious catalytic effect on glucose. We can draw a conclusion that the Mb/GOx on the Ag@Zn-TSA/IL-CPE had an obvious catalysis to H_2O_2, NO_2^- and glucose from the CV graphs.

We further studied in more detail the amperometric current-time response curves

of the two kinds of modified electrodes. Amperometric response of the Mb/Ag@Zn-TSA/IL-CPE to successive addition of H_2O_2 in 0.1 M pH 7.0 PBS was given in **Fig. 5A'**. It was observed that rapid response and sharp increase of Mb/Ag@Zn-TSA/IL-CPE were observed when H_2O_2 was added to the PBS at -0.35 V with the steady-state current obtained within 6 s. The corresponding calibration curve is presented **in the inset of Fig. 5A'** with a linear detection range (LDR) of 0.3 -20000 μM. And the linear regression equation is i(μA)=0.00127c(μM) +4.448 (R=0.9917) with a low detection limit of 0.08 μM (S/N = 3) and a sensitivity of 1.27 $\mu A \cdot mM^{-1}$. **Fig. 5B'** displayed the amperometric response of the Mb/Ag@Zn-TSA/IL-CPE upon successive addition of $NaNO_2$ to 0.1 M pH 7.0 PBS at 0.8 V under stirring. The biosensor exhibited a very rapid and sensitive response to the changes of NO_2^- concentration, the steady-state current being reached in 5 s. Under these conditions, a calibration graph was constructed for NO_2^- (**inset in Fig. 5B'**), with two linear ranges of 1.3 μM -1660 μM and 2262 μM -133000 μM and a low detection limit of 0.5 μM. Two linear ranges were obtained and the fitting regression equations were given as follows: i(μA) = -0.00111c(μM) + 1.855 (R=0.976), i(μA) = -0.0001855c(μM) + 21.321 (R=0.985). **Fig. 5C'** showed a typical current-time plot of our newly developed biosensors on a successive addition of glucose under optimized experimental conditions. The response current was raised quickly and steeply to a stable value when glucose was added into the stirring buffer solution. The response current increased linearly with an increase of glucose concentration and gradually reached a saturation value at a high glucose concentration (see **inset in Fig. 5C'**),

317 which suggested that the active sites of enzyme units were saturated at those glucose
318 levels. In addition, the linear range of the calibration for the glucose response was 2.0
319 μM~1022 μM with a correlation coefficient of 0.995 and a low detection limit of 0.8
320 μM (S/N = 3). Compared with other modified electrodes listed in Table 1, the
321 modified electrode we prepared had wider linear range and lower detection limit,
322 indicating that the immobilized Mb/GOx in Ag@Zn-TSA/IL composite film possess
323 higher enzymatic activity, and the proposed electrodes exhibit a high affinity for H_2O_2,
324 NO_2^- and glucose.

325 **Table 1. here**

326 *3.7 Interference experiment*

327 **Fig. 6. here**

328 The specificity of the Mb/Ag@Zn-TSA/IL-CPE was evaluated at 0.8 V and the
329 GOx/Ag@Zn-TSA/IL-CPE was evaluated at -0.45 V, respectively, by observing the
330 effect of ascorbic acid (AA), glucose and uric acid (UA) on the current value, as
331 shown in **Fig. 6**. The current signal of Mb/Ag@Zn-TSA/IL-CPE **(Fig. 6A**) showed no
332 change in current after the addition of AA (10 μM), glucose (10 μM) and UA (10 μM)
333 in the presence of 50 μM NO_2^- at intervals between 300 and 350 s, which showed a
334 high selectivity for a NO_2^- substrate. For the amperometric measurement of
335 GOx/Ag@Zn-TSA/IL-CPE, at an applied potential of -0.45 V **(Fig. 6B**), the
336 GOx/Ag@Zn-TSA/IL-CPE showed no change in current after the addition of AA (5
337 μM), NO_2^- (5 μM) and UA (5 μM) in the presence of 50 μM glucose at intervals

between 750 and 950 s, which showed a high selectivity for a glucose substrate.

3.8 Real samples analysis

To further investigate the potential application of the sensor for practical analysis, the sensors were used to test the recovery of different concentrations of H_2O_2 and glucose in human serum samples. Before detection of H_2O_2 and glucose, the human serum samples were diluted 200 times by 0.1 M pH 7.0 PBS [38]. Recovery studies were completed by adding standard solution into samples. The obtained results were displayed in Table 2. The results showed that the proposed sensor could be preliminarily applied in the determination of H_2O_2 and glucose in human serum samples.

Table 2. here

3.9 Stability and reproducibility of modified electrodes

In the range of 0.2 V ~ -0.8 V, the scanning rate of 0.1 $V \cdot s^{-1}$ was used to continuous scanning until the cyclic voltammogram was not significantly changed. The stability and reproducibility of Mb/Ag@Zn-TSA/IL-CPE were investigated by CVs. The reproducibility of Mb modified electrode was showed by comparing the response currents of eight modified electrodes fabricated one time, and the RSD was 5% in 0.1 M pH 7.0 PBS, indicating that the reproducibility of the modified electrode was excellent. The as-prepared Mb/Ag@Zn-TSA/IL-CPE retained 95% of its initial response after in 0.1 M PBS (pH 7.0) at 4□ for 2 weeks and maintained 83% of its initial activities after 4 weeks, Likewise, the RSD of GOx/Ag@Zn-TSA/IL-CPE was

4% in 0.1 M pH 7.0 PBS, and GOx modified electrode retained 87% of its initial response after in 0.1 M PBS (pH 7.0) at 4℃ for 2 weeks and maintained 78% of its initial activities after 4 weeks, indicating that the Mb/GOx modified electrode showed a better stability and reproducibility.

4. Conclusion

A novel multi-function Ag@Zn-TSA was prepared as highly efficient immobilization matrixes of Mb/GOx for electrochemical biosensing. Spectroscopic and electrochemical examinations revealed that the Ag@Zn-TSA composite was biocompatible matrix for immobilizing Mb/GOx, which showed good stability and bioactivity. The outcome of this demonstrated that the Ag@Zn-TSA composite could effectively immobilize Mb/GOx and facilitate the electron transfer between Mb/GOx and underlying electrode, as well as had an obvious catalytic effect on the small molecule (NO_2^-, H_2O_2, glucose). The proposed sensor exhibits wide linear range, high sensitivity, low detection limit, good stability and reproducibility. Thus, Ag@Zn-TSA was a kind of ideal material as highly efficient immobilization matrixes for sensitive electrochemical biosensing. In addition, the characteristics of MOFs composites could make them as promising materials in constructing wide range of sensing interface, and extend the scope of applications on electrochemical sensors.

Acknowledgments

The authors appreciate the support from the National Natural Science Foundation of China (No. 21575111), the Projects in the National Science & Technology (No.

2012BAC04B02), the Overall Innovation Project of Science & Technology in Shaanxi Province (No. 2011KTCG03-07).

Appendix A. Supplementary material

Supplementary material related to this article can be found at http://….

References

[1] S. Ray, S. Chand, Y. B. Zhang, S. Nussbaum, K. Rajeshwar, R. Perera, Implications of active site orientation in myoglobin for direct electron transfer and electrocatalysis based on monolayer and multilayer covalent immobilization on gold electrodes, Electrochim. Acta. 99 (2013) 85-93.

[2] E. Koposova, G. Shumilova, Y. Ermolenko, A. Kisner, A. Offenhäusser, Y. Mourzina, Direct electrochemistry of cytc and hydrogen peroxide biosensing on oleylamine- and citrate-stabilized gold nanostructures, Sens. Actuators, B. 207 (2015) 1045-1052.

[3] S. Y. Dong, N. Li, T. L. Huang, H. S. Tang, J. B. Zheng, Myoglobin immobilized on LaF_3 doped CeO_2 and ionic liquid composite film for nitrite biosensor, Sens. Actuators, B. 173 (2012) 704-709.

[4] Y. X. Piao, D. J. Han, T. S. Seo, Highly conductive graphite nanoparticle based enzyme biosensor for electrochemical glucose detection, Sens. Actuators, B. 194 (2014) 454– 459.

[5] X. B. Lu, Q. Zhang, L. Zhang, J. H. Li, Direct electron transfer of horseradish peroxidase and its biosensor based on chitosan and room temperature ionic

liquid, Electrochem. Commun. 8 (2006) 874–878.

[6] A. Dhakshinamoorthy, H. Garcia, Metal-organic frameworks as solid catalysts for the synthesis of nitrogen-containing heterocycles, Chem. Soc. Rev. 43 (2014) 5750–5765.

[7] X. H. Liu, J. G. Ma, Z. Niu, G. M. Yang and P. Cheng, An Efficient Nanoscale Heterogeneous Catalyst for the Capture and Conversion of Carbon Dioxide at Ambient Pressure, Angew. Chem. Int. Ed. 54(3) (2015) 988-991.

[8] G. S. Yang, Z. L. Lang, H. Y. Zang, Y. Q. Lan, W. W. He, X. L. Zhao, L. K. Yan, X. L. Wang and Z. M. Su, Control of interpenetration in S-containing metal-organic frameworks for selective separation of transition metal ions, Chem. Commun. 49(11) (2013) 1088-1090.

[9] P. Xu, X. Li, H. Yu and T. Xu, Advanced Nanoporous Materials for Micro-Gravimetric Sensing to Trace-Level Bio/Chemical Molecules, Sensors, 14(10) (2014) 19023-19056.

[10] X. Wang, X. B. Lu, L. D. Wu and J. P. Chen, 3D metal-organic framework as highly efficient biosensing platform for ultrasensitive and rapid detection of bisphenol A, Biosens. Bioelectron. 65 (2015) 295-301.

[11] W. W. Zhan, Q. Kuang, J. Z. Zhou, X. J. Kong, Z. Xie and L. S. Zheng, Semiconductor @ metal-organic framework core-shell heterostructures: a case of ZnO@ZIF-8 nanorods with selective photoelectrochemical response, J. Am. Chem. Soc. 135 (2013) 1926-1933.

[12] H. Hosseini, H. Ahmar, A. Dehghani, A. Bagheri, A. Tadjarodi and A. Fakhari,

A novel electrochemical sensor based on metal-organic framework for electro-catalytic oxidation of L-cysteine, Biosens. Bioelectron. 42 (2013) 426-429.

[13] D. Fernandes, A. S. Barbosa, J. Pires, S. Balula, L. C. Silva and C. Freire, Novel Composite Material Polyoxovanadate@MIL-101(Cr): A Highly Efficient Electrocatalyst for Ascorbic Acid Oxidation, Appl. Mater. Interfaces.5(24) (2013) 13382-13390.

[14] Y. Wang, H. Ge, Y. C. Wu, G. Q. Ye, H. H. Chen and X. Y. Hu, Construction of an electrochemical sensor based on amino-functionalized metal-organic frameworks for differential pulse anodic stripping voltammetric determination of lead, Talanta, 129 (2014) 100-105.

[15] V. Lykourinou, Y. Chen, X. S. Wang, L. Meng, T. Hoang, L. J. Ming, R. L. Musselman, S. Q. Ma, Immobilization of MP-11 into a mesoporous metal-organic framework, MP-11@mesoMOF: a new platform for enzymatic catalysis, J. Am. Chem. Soc. 133 (2011) 10382–10385.

[16] H. Hosseini, H. Ahmar, A. Dehghani, A. Bagheri, A. R. Fakhari, M. M. AminiD, Au-SH-SiO_2 nanoparticles supported on metal-organic framework (Au-SH-SiO_2@Cu-MOF) as a sensor for electrocatalytic oxidation and determination of hydrazine, Electrochim. Acta. 88 (2013) 301-309.

[17] S. Shahrokhian, N. H. Nassab, Nanodiamond Decorated with Silver Nanoparticles as a Sensitive Film Modifier in a Jeweled Electrochemical Sensor: Application to Voltammetric Determination of Thioridazine, Electroanalysis. 25

(2013) 417-425.

[18] S. Shahrokhian, S. Ranjbar, and M. Ghalkhani, Modification the Electrode Surface by Prepared Ag Nanoparticles Decorated Nano Diamond-Graphite Modified Electrode for Voltammetric Determination of Ceftizoxime, Electroanalysis, 27 (2015) 1-9.

[19] Y. Li, H. J. Schluesener, S. Xu, Gold nanoparticle-based biosensors, Gold Bull. 43 (2010) 29-41.

[20] X. F. Wu, Z. B. Bao, B. Yuan, J. Wang, Y. Q. Sun, H. M. Luo, S. G. Deng,Microwave synthesis and characterization of MOF-74 (M = Ni, Mg) for gas separation, Microporous Mesoporous Mater. 180 (2013) 114-122.

[21] H. Yang, J. Z. Zhao, L. Z Song, L. C. Shen, Z. C. Wang, L. Wang, D. Zhang, Photoluminescent properties of ZnS: Mn nanocrystals prepared in inhomogeneous system, Mater. Lett. 57(15) (2003) 2287-2291.

[22] F. W. T. Goha, Z. L. Liu, X. M. Ge, Y. Zong, G. J. Du, T. S. A. Hor, Ag nanoparticle-modified MnO_2 nanorods catalyst for use as an air electrode in zinc-air battery, Electrochim. Acta, 114 (2013) 598-604.

[23] H. T. Liu, J. S. Zhong, X. J. Liang, J. F. Zhang, W. D. Xiang, A mild biomolecule-assisted route for preparation of flower-like $AgBiS_2$ crystals, J. Alloys Compd. 509 (2011) L267-L272.

[24] E. Lojou, M. T. Giudici-Orticoni, P. Bianco, Direct electrochemistry and enzymatic activity of bacterial polyhemic cytochrome c incorporated in clay films, J. Electroanal. Chem. 579 (2005) 199-213.

[25] E. V. Ivnova, E. Magner, Direct electron transfer of haemoglobin and myoglobin in methanol and ethanol at didodecyldimethylammoniumbromide modified pyrolytic graphite electrodes, Electrochem. Commun. 7 (2005) 323-327.

[26] X. J. Liu, L. B. Shang, Z. Y. Sun, G. X. Li, Direct electrochemistry of hemoglobin in dimethyldioctadecyl ammonium bromide film and its electrocatalysis to nitric oxide, J. Biochem. Biophys. Methods, 62 (2005) 143-151.

[27] Y. Lvov, H. Mohwald, In protein architechture: Interfacing Molecular Assemblies and Immobilization Biotechnology, Marcel Dekker, New York, (2000) 125-166.

[28] J. F. Rusling, Enzyme bioelectrochemistry in cast biomembrane-like films, Acc. Chem. Res. 31 (1998) 363-369.

[29] X. J. Chen, Z. X. Chen, J. W. Zhu, C. B. Xu, W. Yan, C. Yao, A novel H_2O_2 amperometric biosensor based on gold nanopariticles/self-doped polyaniline nanofibers, Biosens. Bioelectron. 82 (2011) 87-94.

[30] F. S. Yardimci, M. Senel, A. Baykal, Amperometric hydrogen peroxide biosensor based on cobalt ferrite-chitosan nanocomposite, Mater. Sci. Eng. C, 32 (2012) 269-275.

[31] K. F. Zhou, Y. H. Zhu, X. L. Yang, J. Luo, C. Z. Li, S. R. Luan, A novel hydrogen peroxide biosensor based on Au-graphene-HRP-chitosan biocomposites, Electrochim. Acta. 55 (2010) 3055-3060.

[32] R. Yue, Q. Lu, Y. K. Zhou, A novel nitrite biosensor based on single-layer grapheme nanoplatelet-protein composite film, Biosens. Bioelectron. 26, (2011) 4436-4441.

[33] W. Sun, X. Q. Li, K. Jiao, Direct Electrochemistry of Myoglobin in a Nafion-Ionic LiquidComposite Film Modified Carbon Ionic Liquid Electrode, Electroanalysis. 21 (2009) 959-964.

[34] W. Sun, X.Q. Li, P. Qin, K. Jiao, Electrodeposition of Co nanopariticles on the carbon ionic liquid electrode as a platform for myoglobin electrochemical biosensor, J. Phys. Chem. C. 113 (2009) 11294-11300.

[35] S. Y. Deng, G. Q. Jian, J. P. Lei, Z. Hu, H. X. Ju, A glucose biosensor based on direct electrochemistry of glucose oxidase immobilized on nitrogen-doped carbon nanotubes, Biosens. Bioelectron. 25 (2009) 373-377.

[36] N. German, A. Ramanavicius, A. Ramanaviciene, Electrochemical deposition of gold nanoparticles on graphite rod for glucose biosensing, Sens. Actuators, B. 203 (2014) 25-34.

[37] J. H. Li, D. Z. Kuang, Y. L. Feng, F. X. Zhang, M. Q. Liu, Glucose biosensor based on glucose oxidase immobilized on a nanofilm composed of mesoporous hydroxyapatite, titanium dioxide, and modified with multi-walled carbon nanotubes, Microchim Acta, 176 (2012) 73-80.

[38] J. L. Liu, L. L. Lu, A. Q. Li, J. Tang, S. G. Wang, S. Y. Xu, L. Y. Wang, Simultaneous detection of hydrogen peroxide and glucose in human serum with upconversion luminescence, Biosens. Bioelectron, 68 (2015) 204–209.

Table 1. Comparison with other modified electrodes

Biosensor		Detection range (μM)	Detection limit (μM)	Reference
Au-SPAN/HRP/GCE	H_2O_2	10-2000	1.6	[29]
GCE/Chi/$CoFe_2O_4$/HRP	H_2O_2	30-8000	2.0	[30]
Au/GS/HRP/CS	H_2O_2	5.0-5130	1.7	[31]
IL/Mb/Ag@Zn-TSA-CPE	H_2O_2	0.3-20000	0.15	This work
Nafion/SLGnP-TPA-GOx	NO_2^-	50-2500	10	[32]
Nafion–$BMIMPF_6$/GOx/CILE	NO_2^-	100-8400	50	[33]
Nafion/GOx/MWCNTs/CILE	NO_2^-	8.0-196	6.0	[34]
IL/Mb/Ag@Zn-TSA-CPE	NO_2^-	1.3-133000	0.5	This work
GOx/CNx-MWNTs	glucose	20-1020	10	[35]
GOx/Au-NPs/graphite	glucose	100-10000	80	[36]
GOx/Meso-HAP/Meso-TiO_2/MWCNT	glucose	10-15200	2.0	[37]
IL/GOx/Ag@Zn-TSA-CPE	glucose	2.0 -1022	0.8	This work

Tabel 2. Test for recovery of H_2O_2 and glucose

	Samples	Added c / (μM)	Determined c / (μM)	Recovery (%)	RSD (%)
human serum (H_2O_2)	1	100	98.4	98.4	2.6
	2	300	311.3	103.6	4.3
	3	500	512.7	102.4	3.7
human serum (glucose)	1	100	101.2	101.2	3.4
	2	300	307.2	102.3	4.5
	3	500	503.6	100.6	4.7

Figure Captions

Scheme 1. Schematic diagram of the procedure to synthesize Zn-TSA and Ag@Zn-TSA

Fig. 1. (A) FT-IR spectra of Zn-TSA material and TSA; (B) XRD pattern of Ag@Zn-TSA composite and silver standard card; (C) SEM images of (1) Zn-TSA, (2) Ag@Zn-TSA; (D) EDS images of Ag@Zn-TSA.

Fig.2. Electrochemical impedance spectra (EIS) of (A) Ag@Zn-TSA-CPE, Mb/Ag@Zn-TSA-CPE, Mb/Ag@Zn-TSA/IL-CPE (B) Zn-TSA-CPE, Ag@Zn-TSA-CPE, GOx/Ag@Zn-TSA-CPE, GOx/Ag@Zn-TSA/IL-CPE in 5.0 mM $[Fe(CN)_6]^{3-/4-}$ (1:1) solution containing 0.1 M KCl. Inset shows the EIS of CPE. The parameters were as follows: frequency range from 0.01 Hz to 10^5 Hz; initiative potential, 0.2 V; amplitude, 0.01 V and quiet time of 2 s.

Fig. 3. (A) Cyclic voltammograms (CVs) of (a) CPE, (b)Mb/IL-CPE, (c) Mb/Zn-TSA/IL-CPE, (d) Mb/Ag@Zn-TSA/IL-CPE. (B) CVs of (a') GOx-CPE (b')GOx/IL-CPE, (c') GOx/Zn-TSA/IL-CPE, (d') GOx/Ag@Zn-TSA/IL-CPE. Supporting solution: 0.1 M pH 7.0 PBS, scan rate: 100 $mV \cdot s^{-1}$.

Fig. 4. Cyclic voltammograms (CVs) of (A) Mb/Ag@Zn-TSA/IL-CPE (B) GOx/Ag@Zn-TSA/IL-CPE in 0.1M pH 7.0 PBS at various scan rates: 20, 50, 80, 100, 150, 200, 250, 300, 350, 400, 450, 500, 600, 700, 800, 900 and 1000 $mV \cdot s^{-1}$. Insets show the plots of cathodic and anodic peak currents vs. (a) scan rates and (b) square root of scan rates; (A') and (B') Linear relationship of redox peak potential (Ep,a and Ep,c) vs. natural logarithm (lnv).

Fig. 5. Cyclic voltammograms of (A) Mb/Ag@Zn-TSA/IL-CPE, (B) Mb/Ag@Zn-TSA/IL-CPE, (C) GOx/Ag@Zn-TSA/IL-CPE in 0.1M pH 7.0 PBS containing different concentration of H_2O_2 (a-c: $0\sim5.00\times10^{-3}$ M), NO_2^- (a-d: $0\sim5.00\times10^{-3}$ M), glucose (a-d: $0\sim2.5\times10^{-3}$ M) at scan rate 100 $mV \cdot s^{-1}$, respectively. Amperometric current-time response curves of (A') Mb/Ag@Zn-TSA/IL-CPE, (B') Mb/Ag@Zn-TSA/IL-CPE, (C') GOx/Ag@Zn-TSA/IL-CPE upon successive addition of H_2O_2, NO_2^-, glucose into pH 7.0 PBS solution, respectively. Applied potential: -0.35 V (A'), 0.8 V (B'), -0.45 V (C'). Inset: calibration curve of steady-state currents vs. H_2O_2, NO_2^- and glucose concentration at Mb/Ag@Zn-TSA/IL-CPE, Mb/Ag@Zn-TSA/IL-CPE and GOx/Ag@Zn-TSA/IL-CPE, respectively.

Fig. 6. (A) Amperometric current-time response curves of Mb/Ag@Zn-TSA/IL-CPE upon successive addition of 25 μM NO_2^-, 10 μM ascorbic acid, 10 μM glucose, 10 μM uric acid into pH 7.0 PBS solution at a detection potential of 0.8 V. (B) Amperometric current-time response curves of GOx/Ag@Zn-TSA/IL-CPE upon successive addition of 25 μM glucose, 5.0 μM ascorbic acid, 5.0 μM NO_2^-, 5.0 μM uric acid into pH 7.0 PBS solution at a detection potential of -0.45 V.

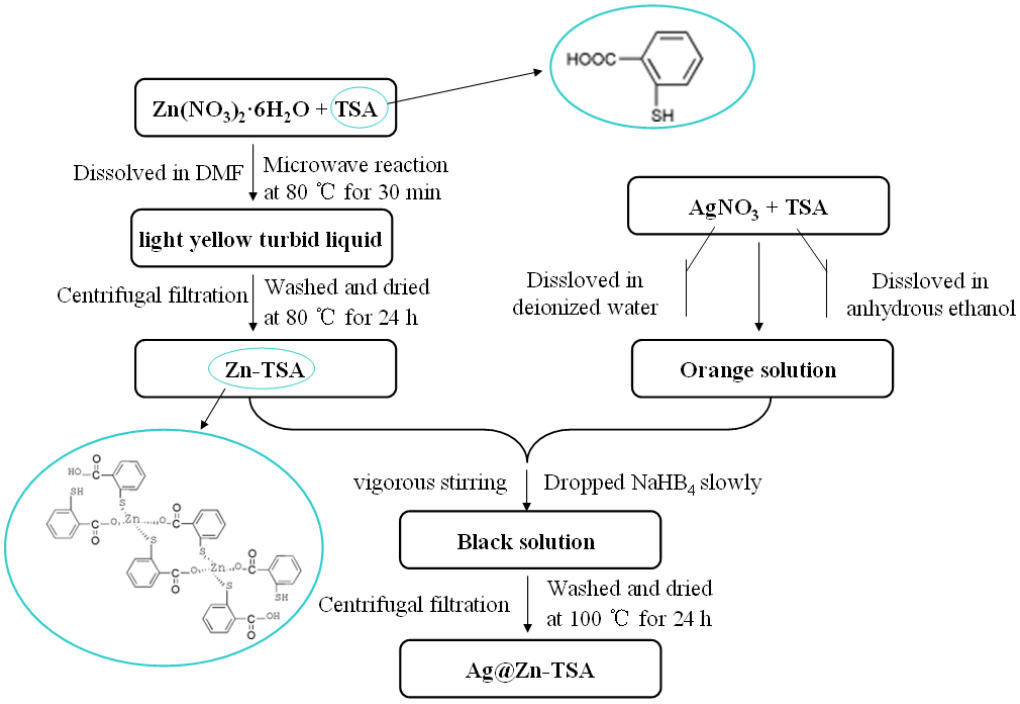

Scheme 1

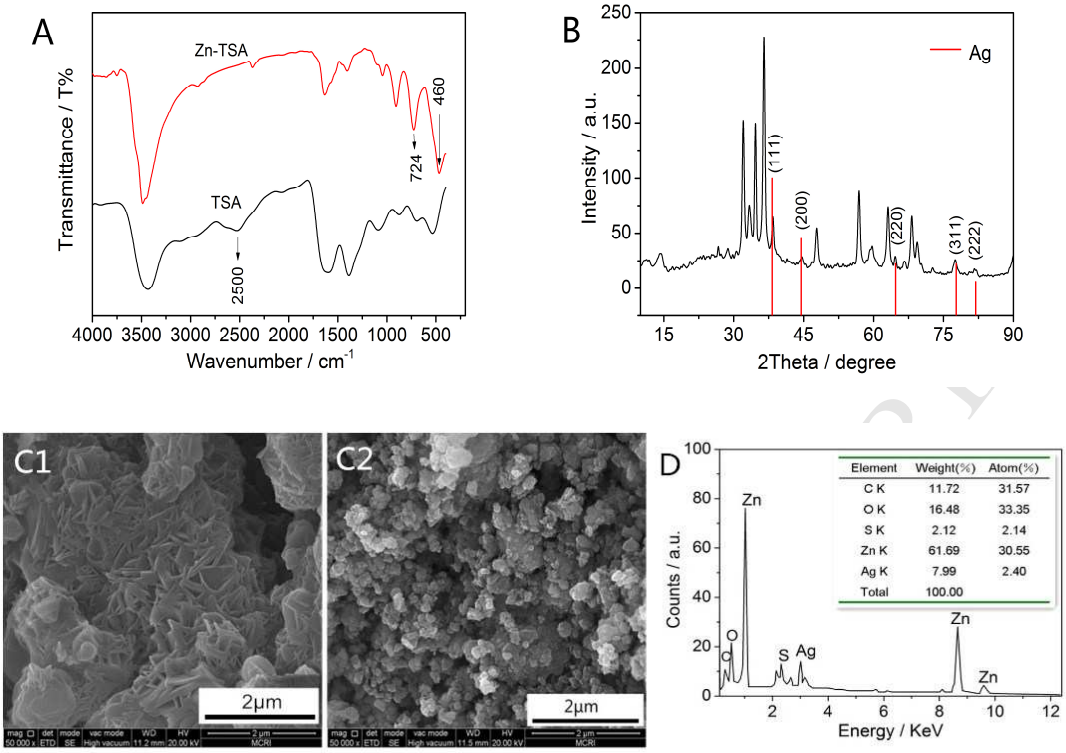

Fig. 1

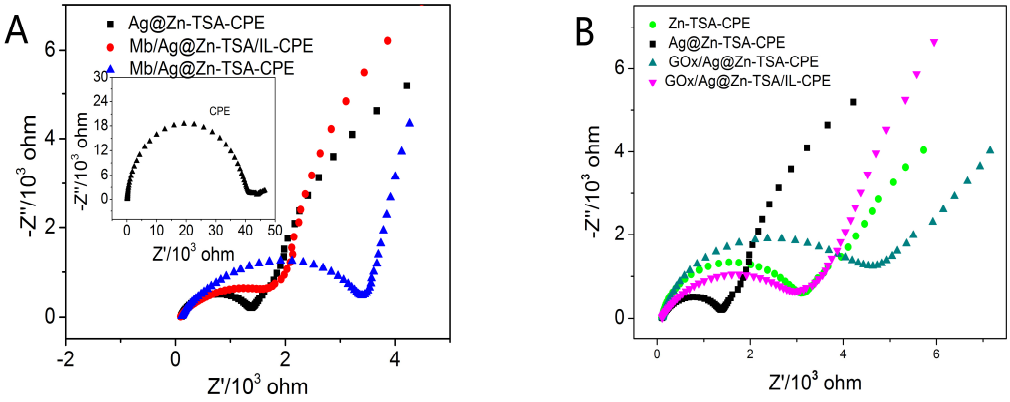

Fig. 2

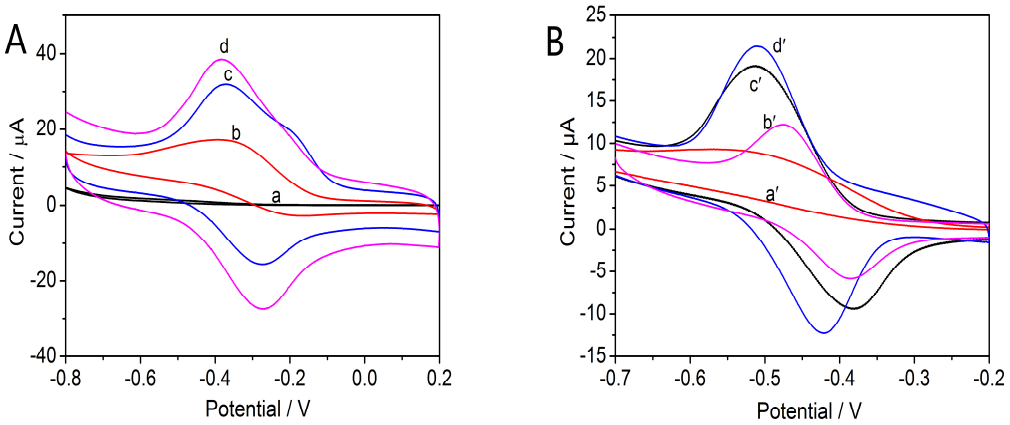

Fig. 3

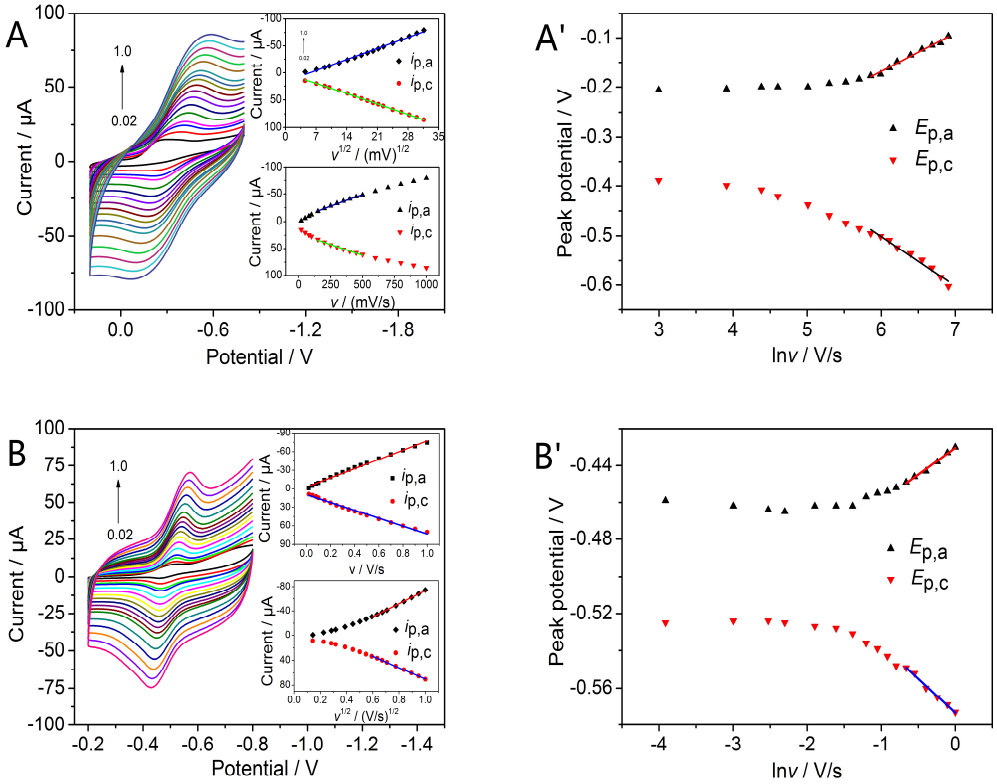

Fig. 4

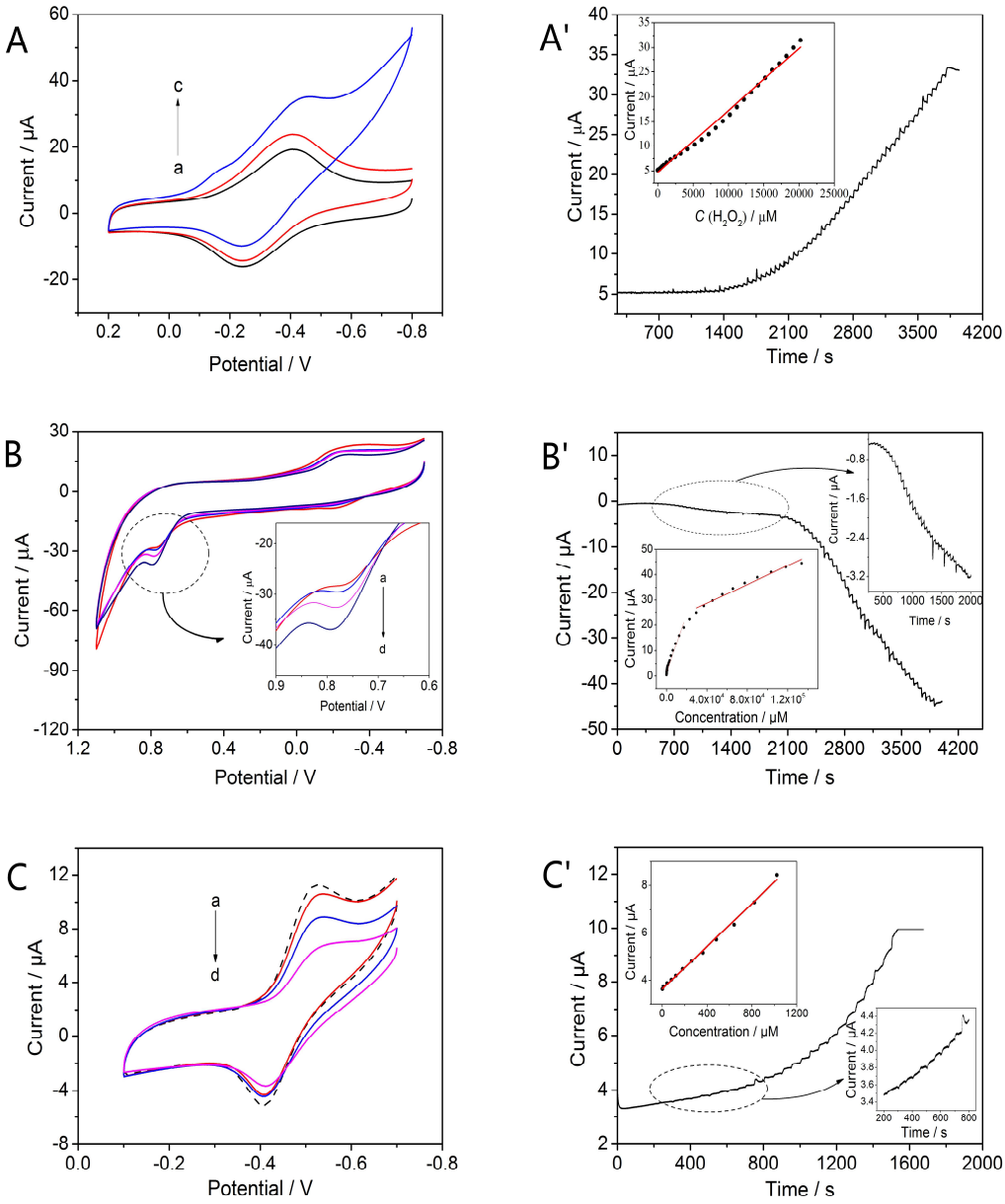
A
Current / μA
Potential / V
c
a
A'
Current / μA
Time / s
C (H2O2) / μM
B
Current / μA
Potential / V
a
d
B'
Current / μA
Time / s
Concentration / μM
C
Current / μA
Potential / V
a
d
C'
Current / μA
Time / s
Concentration / μM

Fig. 5

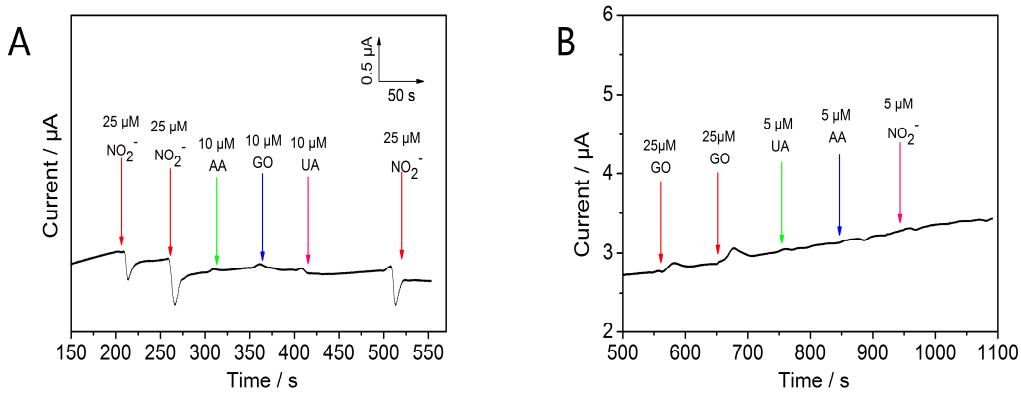

Fig. 6

Highlights

1. Novel Ag@Zn-TSA was used as highly efficient immobilization matrixes of Mb/glucose.
2. We exploited multi-function MOFs for a wide range of electrocatalytic sensing interface.
3. The proposed biosensors had an excellent catalytic effect on the small molecule (NO_2^-, H_2O_2, glucose).